Demonstrating LS-DYNA®'s Capabilities in Welding Simulations by Experiments

Maarten Rikken
Arup, Infrastructure, The Netherlands
Gianmarco Montalbini
Arup, Specialist Technology and Research, United Kingdom
Bruna Frydman
Arup, Specialist Technology and Research, United Kingdom
David Gration
Arup, Specialist Technology and Research, United Kingdom

Abstract

*This study examines the welding residual stress formation in a bead-on-plate welded specimen using LS-DYNA and a series of physical experiments to validate the simulation approach. Calculating residual stresses numerically could be used to improve welding procedures or to assess the structural integrity of welded joints in service conditions. Dilatometer and tensile tests at elevated temperature were conducted to obtain thermal expansion behavior and stress-strain curves of the S355G10+M base material. The software package JMatPro provided the other material properties required for the welding simulations in LS-DYNA. A thermal analysis was set up in LS-DYNA to simulate a bead-on-plate welded specimen for which the weld heat input was modelled with the Goldak heat flux distribution. Welding experiments were carried out and the transient temperature distribution during welding was measured with thermocouples. This was used to calibrate the thermal analysis in LS-DYNA. Macrographs of the welded specimen helped to validate the fusion zone shape and cooling rate in the heat affected zone. The thermal analysis results were subsequently coupled with a mechanical analysis to calculate the thermal strains and residual stress formation. *MAT_270/CWM was used for this analysis as it is able to reproduce the transient weld material deposition. The residual stress over the full depth of the specimen was compared to the experimentally obtained residual stress state. The crack compliance method was used to experimentally measure the residual stress over the full depth of the specimen. The numerically and experimentally determined residual stress distributions are in good agreement. This study demonstrates the capabilities of LS-DYNA to simulate welding procedures and validates the corresponding results using physical experiments.*

Introduction

Welding is a manufacturing process that connects structural elements, mostly metals. Many applications of welding are used worldwide across various industries. One of the most common welding techniques is arc welding, in which an electric arc is struck between the tip of the welding torch and the workpiece. A filler material is continuously fed into the hot arc where both the filler and base material become molten. A welded joint is created after solidification. Several passes of the welding torch may be required to deposit sufficient material.

Metals have temperature dependent material properties in which both their stiffness and strength decay at elevated temperature. Due to thermal expansion and contraction metals also develop thermal strains during a welding procedure which, together with changing mechanical material properties, promotes the formation of residual stresses and distortions. Phase transformations in the heat affected zone influence strength, ductility and toughness if the material is sufficiently heated during the welding procedure. This can lead to weld imperfections, e.g. cracks, that could compromise the fatigue and strength performance of the joint.

Welding procedures are largely developed by experience and expert judgement in which the above-mentioned unfavorable side effects are reduced to a minimum. Execution standards and appropriate qualifications of welders are also necessary to control weld quality. Poor welding procedures and practices can lead to costly and time-consuming repairs if they are noticed. However, if not noticed they could lead to a reduction in capacity, compared to the design expectation, leading to unsafe conditions or premature failure.

Numerical modelling techniques are now available to simulate welding processes. The full welding procedure being modelled using a thermo-mechanical coupled analysis. Various heat sources are applied for different welding procedures, Goldak's heat source [1] is the most common representation for arc welding processes. This is based on a three-dimensional transient heat flux distribution representing the moving weld arc that locally melts the base and filler material. The change in temperature across the workpiece can be numerically studied using this heat source, thermal material properties and thermal boundaries.

A subsequent mechanical analysis uses the thermal analysis results to calculate thermal strains, stresses and distortions. The thermal expansion and metallurgical phase transformation behavior of the material couple the thermal and mechanical analysis. The non-uniform expansion of the welded workpiece and the strength-stiffness characteristics of the cooler, surrounding metal generate residual stresses and distortions. The fusion and heat affected zone are additionally affected by phase transformations as they are sufficiently heated to allow for iron lattice structure transformations. The relationship between material, thermal and mechanical aspects in welding simulations is shown in Figure 1 and Table 1.

LS-DYNA has built in capabilities for welding simulations including material and temperature loading cards. In this paper, the welding simulation capabilities of LS-DYNA are validated by comparison with physical experiments. A bead-on-plate welding experiment using a S355G10+M steel grade was simulated in LS-DYNA, using material properties obtained from a commercially available software package JMatPro. The thermal and mechanical analysis results were validated by means of experiments, demonstrating the capabilities of LS-DYNA in welding simulations.

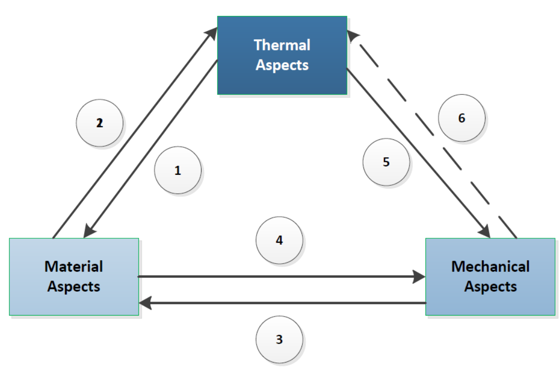

Figure 1 The three aspects and their relation for welding simulations

Table 1 Explanation of the different relationships in welding simulations

Relations between the different aspects for welding simulations	
1.	Thermal material properties are temperature dependent in which the thermal distribution determines phase transformations
2.	Temperature distribution depends on the material properties.
3.	Loading conditions determine material properties (i.e. creep, cyclic thermo-mechanical loading etc.).
4.	Mechanical material properties translate the temperature increments into thermal strains, residual stresses, phase transformations and distortions.
5.	The transient temperature distribution is used in the mechanical analysis as load input.
6.	Plastic strain development within a material creates heat.

Material data

The 50mm thick S355G10+M base material had been manufactured by a thermo-mechanical rolling treatment. The microstructure consists of coarse pearlite grains in a ferritic matrix. The average grain size is 22.1 µm and the average Vickers Hardness is 175 HV. A Union BA 70 wire was used as a filler material. The chemical composition is shown in Table 2, this was obtained by optical emission spectroscopy. It is assumed that the base and filler material have similar material properties. This assumption is justified due to the small fusion zone in this weld and the fact that the chemical composition is comparable between the base and filler material.

Table 2 Chemical composition of the base and wire material

	C	**Mn**	**Si**	**S**	**P**	**Al**	**N**	**Cu**	**Ni**	**Cr**	**Nb**	**Ti**	**As,Sn,Mo,V,B**	**Fe**
Base	0.09	1.34	0.293	0.002	0.013	0.031	0.005	0.239	0.240	0.024	0.026	0.017	≤0.002	rest
Wire	0.06	1.40	0.450	≤0.02	≤0.02									rest

Welding simulations require temperature dependent thermal and mechanical material properties. Java-Based Material Properties (JMatPro) provides thermal-physical material properties, as a function of material type, physical principles and statistical methods [2]. The required input for JMatPro is the chemical composition, austenite grain size and cooling rate of the material. The latter two parameters are not constant across the fusion and heat affected zone and are affected by the thermal history in the actual welding procedures. These parameters were not varied in the simulation reported. In the simulation it was assumed that an austenite grain size of 100 µm and a cooling rate of 1 °C/s is applicable for the entire welded specimen. Ideally the mechanical material properties would be made dependent on the grain size and cooling rate, to capture the changing material properties (i.e. strength, ductility) due to the heat treatment. Although possible in LS-DYNA, this requires an extensive material data set.

The thermal conductivity, specific heat and density of the S355G10+M material are shown in Figure 2. They are included in the material card *MAT_THERMAL_CWM, which is specifically set up for Computational Welding Mechanics (CWM). The mechanical material properties are shown in Figure 3 and were included in material card *MAT_270_CWM. JMatPro presents stress-strain curves for about every 50 degrees Celsius, which are not shown in this paper due to excessive amount of data. The mechanical material card also contains specific input parameters for welding simulations which are discussed below.

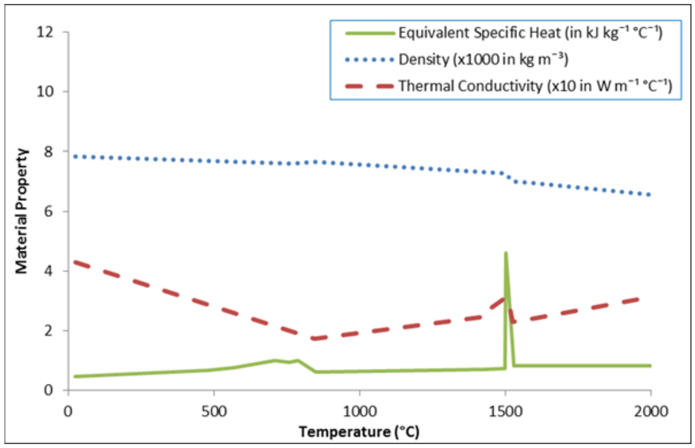

Figure 2 Thermal material properties of the S355G10+M base material

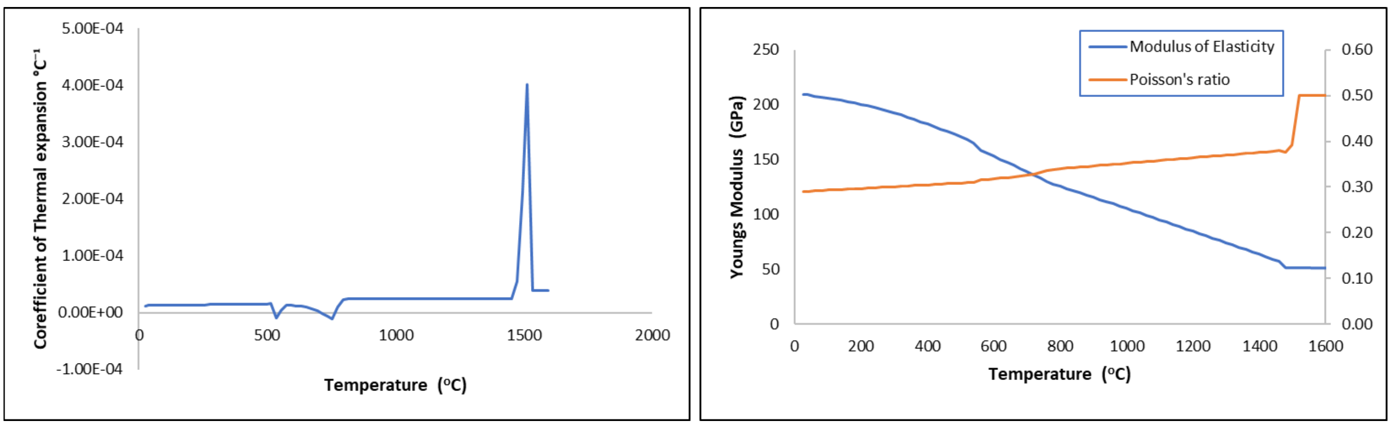

Figure 3 Mechanical material properties of the S355G10+M base material

The filler material is often deposited in several layers during an actual welding procedure, to create the desired joint geometry after solidification. In LS-DYNA, the user models the final weld geometry. Each individual weld pass is then simulated in the software, using a heat source distribution for each weld bead. The weld material that is yet to be deposited does not influence the thermal and mechanical analysis because LS-DYNA includes dead, ghost and normal elements:

- Normal: Base material and weld material that is already deposited
- Ghost: Current weld run in which the elements are activated to normal elements once they reach a predefined temperature level. In the current paper, the liquidus temperature of steel is used; 1530°C
- Dead: Weld beads which are not yet deposited. They are activated to ghost element at a user defined time interval, corresponding to the actual welding procedure specification. A single weld-pass is examined in the current paper and therefore dead elements are not used.

Ghost and dead elements are assigned effectively null material properties. In the current paper, a thermal conductivity of 1E-7 W m^{-1} °C^{-1} and a Young's Modulus of 5000 MPa was used for the ghost elements. These parameters were established in such a way that the ghost elements do not interfere with the active elements in terms of either thermal and/or mechanical response.

Thermal analysis

Four bead-on-plate welding physical experiments were conducted using a gas metal arc welding procedure. The base material plate dimensions were 310x150x50 mm as shown in Figure 4. The weld torch moved along the workpiece with a weld speed of 6.3mm/s. The heat input was 247 amperes and 28.4 volts for all four welding experiments. Weld run on and off plates were used to remove the effects of weld start and finish positions on the bead-on-plate specimen.

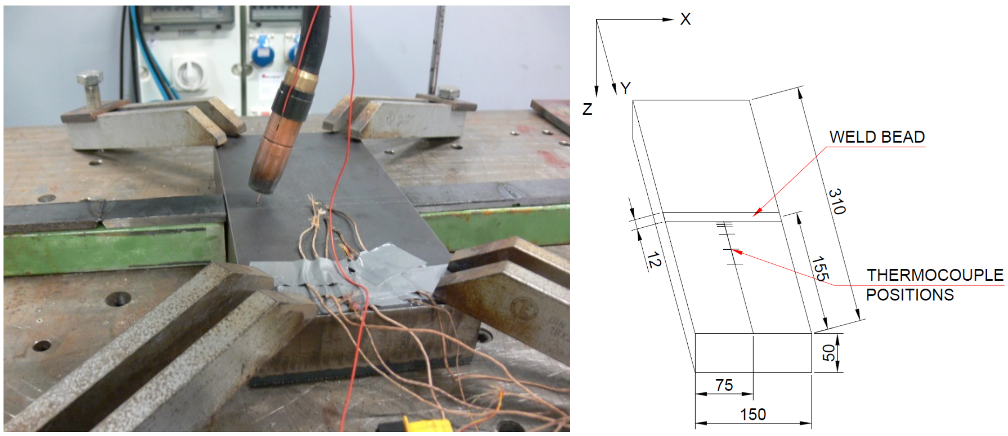

Figure 4 Bead-on-plate welding experiment

Six thermocouples were attached to the workpiece at 2, 5, 10, 20, 40 and 60mm from the weld toe at the weld bead center line. They recorded the temperature during the welding experiments and were used to validate the thermal analysis in LS-DYNA.

The finite element model of the bead-on-plate specimen uses 8-noded fully integrated solid elements with a typical mesh size of 1mm in the area of the weld bead, progressively coarsening to approximately 9mm in the area at the edges of the specimen. Along the welding direction the solid elements have a constant width of 5mm. The full extent of the test specimen has been modelled, with dimensions as indicated in Figure 5.

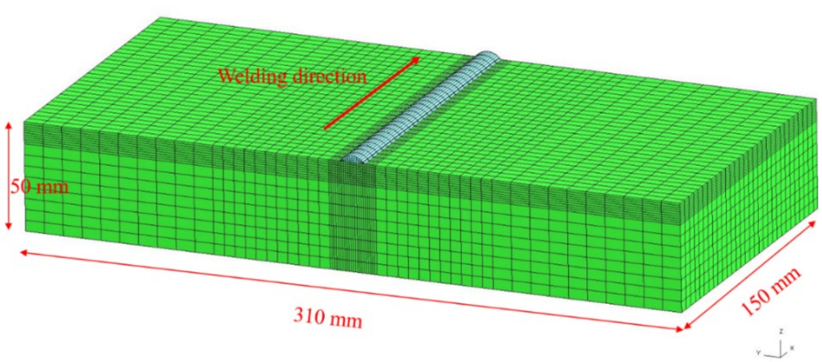

Figure 5 Numerical model in LS-DYNA

The model has two parts (*PART), one for the base plate and one for the elements representing the weld bead. This allows definitions of different thermal and structural properties for the two entities. The plate was not constrained or clamped in any direction during the welding experiments and mechanical boundary conditions were therefore not included in the model. Thermal boundary conditions were assigned to all exterior surfaces with the convection coefficient equal to 5 W mm^{-1} $°C^{-1}$ and the emissivity to 0.7. An initial temperature of 21 °C was assigned to the model.

The transient, volumetric heat flux distribution of Goldak resembles the excited energy by the moving weld arc, as shown in Figure 6. The total heat input, Q (Equation 1), is distributed along two ellipsoidal distributions, expressed in Equations 2 and 3, determining the heat flux at the front $(q_{v,f})$ and rear $(q_{v,r})$ of the heat source center point. The total heat input (Q) is determined by the current (I), voltage (U), weld speed (v) and efficiency (η) of the welding experiment. Goldak's heat source model has therefore a direct coupling to actual welding procedure specifications.

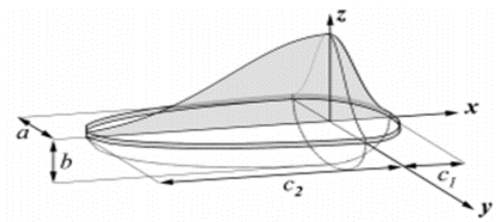

Figure 6 Goldak's volumetric heat flux distribution

$$Q = \frac{\eta U I}{v} \tag{1}$$

$$q_{v,f}(x,y,z,t) = \frac{6\sqrt{3}Qf_f}{abc_1\pi\sqrt{\pi}} e^{-3\left(\frac{x^2}{a^2}+\frac{y^2}{b^2}+\frac{(z-vt)^2}{{c_1}^2}\right)} \tag{2}$$

$$q_{v,r}(x,y,z,t) = \frac{6\sqrt{3}Qf_r}{abc_2\pi\sqrt{\pi}} e^{-3\left(\frac{x^2}{a^2}+\frac{y^2}{b^2}+\frac{(z-vt)^2}{{c_2}^2}\right)} \tag{3}$$

The initial dimensions of the weld pool were measured directly on the macrograph [3] (Figure 7) and are shown below.

- a (semi-width of the ellipsoid) = half of the bead width = 6 mm
- b (depth of the pool) = 3+3 = 6 mm

Furthermore it was taken [4]:

- c_1 = a and c_2 = 2a , as a common assumption
- f_f = 0.8 and f_r = 1.2 (f_f+f_r =2)
- n = 3

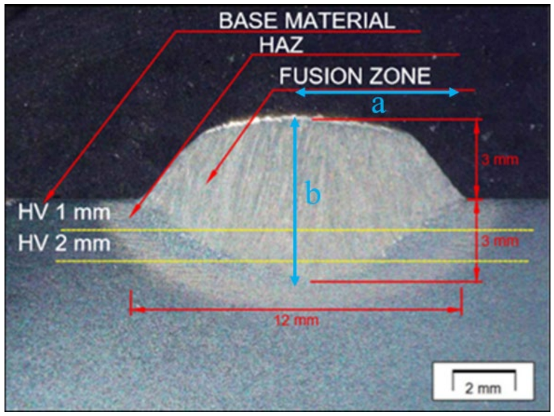

Figure 7 Macrograph of the welded specimen

The Goldak heat source was set up using the *BOUNDARY_WELD_TRAJECTORY card in LS-DYNA.

The left hand image of Figure 10 shows the temperature contour when the weld torch is mid-way along the bead; the welding direction is from left to right. The right hand image shows the elements that have already exceeded the liquidus temperature (1530 °c) and have therefore been activated (in red), while the elements in front of the torch are still in a ghost state (in green).

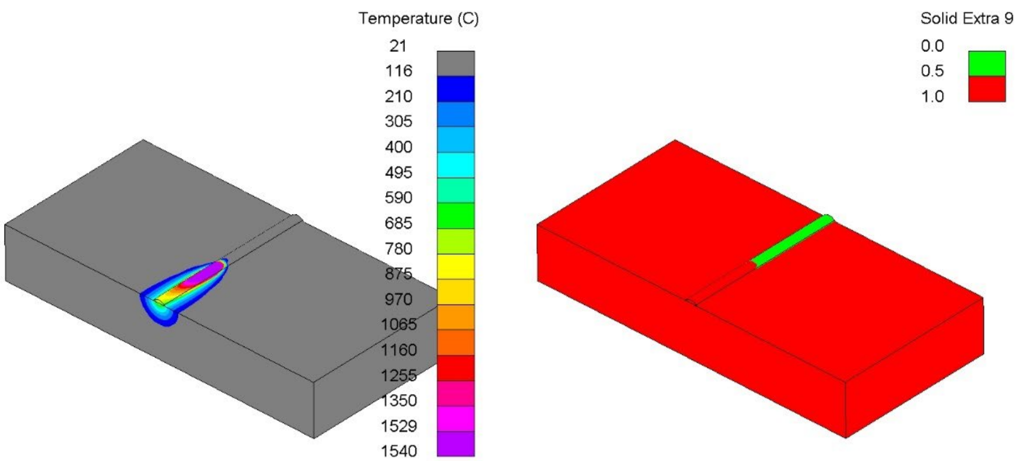

Figure 8 Thermal analysis using Goldak's heat source model

Figure 9 presents both the thermocouple data and the simulated thermal data at the measured temperature locations. The thermocouple data is the average of the four weld experiments. The time t=0 corresponds to the arc ignition time, the temperature was extracted at the specified position from the weld bead centre line. The experimental and numerical temperature output is in good agreement.

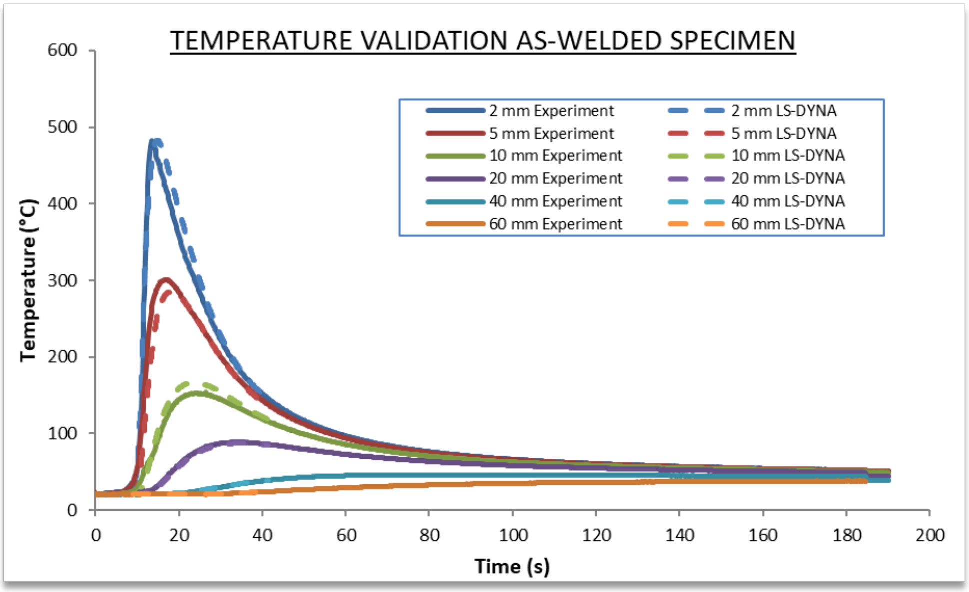

Figure 9 Thermocouple validation of the bead-on-plate welding experiment

The fusion zone is a combination of molten filler and base material and has experienced a temperature of at least the liquidus temperature of steel (1530 °C). Macrographs, including the fusion zone size, are often included in welding procedure specifications. These are therefore a more readily available source of validation data for standard welding simulations than thermocouple data. The fusion zone comparison is shown in Figure 10, the purple contour represents the material that has experienced a temperature exceeding 1530 °C. This corresponds well with the actual fusion zone size.

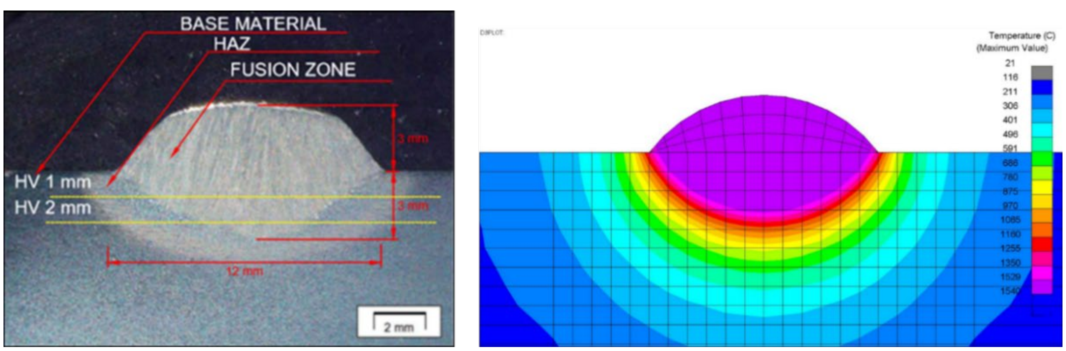

Figure 10 Fusion zone comparison

The thermal analysis presented in this section demonstrates that LS-DYNA is capable of providing an accurate estimation of the thermal flow in the workpiece. The thermal analysis was completed using welding simulation features built-in to LS-DYNA which simplifies the analysis setup.

Mechanical analysis

The crack compliance method was used to experimentally obtain the through thickness residual stress distribution, perpendicular to the weld direction, at 2mm from the weld toe. The 150mm welded specimens were first cut into 25mm sections, it was assumed that the redistribution of the residual stress field by the cutting procedure is negligible. Four strain gauges were placed on the specimens; two at the bottom surface, directly in line with the applied crack, and two gauges at the top surface at 5mm from the crack. A wire electronic discharge machine applied a crack in increments of 0.25mm over the depth of the welded specimens; the fine slit hardly influences the internal stress state in the specimen [5]. The strain gauges measured the stress release after each increment which were then converted to a residual stress field in the uncracked condition. The experiment is shown in Figure 11.

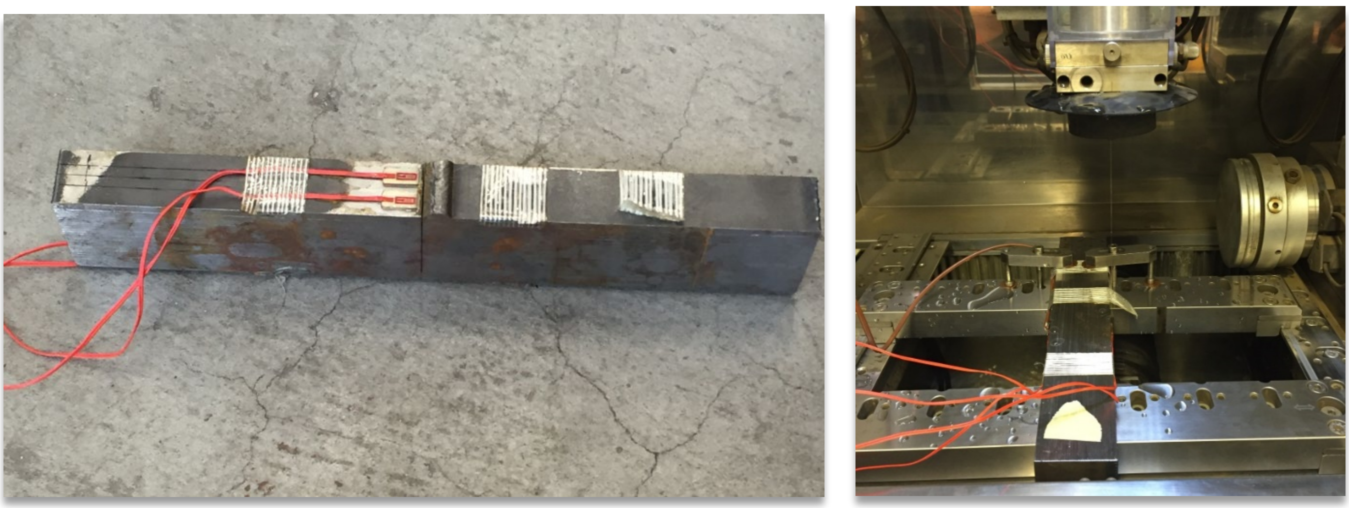

Figure 11 The crack compliance method

A two stage procedure is used to calculate the residual stress field from the strain gauge readings:

1. The stress intensity factor at the crack tip ($K_{rs(a)}$) is calculated by converting the strain increment ($d\varepsilon_m/da$) using Equation 4. The influence function $Z(a)$ is taken from [6] and includes the geometry, crack size, constraint conditions and relative positions of the strain gauges. The constraint condition (E') either assumes plane stress or plane strain conditions.

$$K_{rs(a)} = \frac{E'}{Z(a)}\frac{d\varepsilon_m}{da} \tag{4}$$

2. The second stage uses Bueckner's weight function technique [7] to calculate the residual stress field $\sigma_{rs}(x)$ from the stress intensity factor ($K_{rs(a)}$) using Equation 5. For this, the weight function $\left(h(x,a)\right)$ for a semi-infinite edge crack geometry is taken from Wu and Carlsson [8]. The algorithm presented in [9] is used to invert Equation 5 and to obtain the residual stress field over the full depth of the specimen.

$$K_{rs(a)} = \int_0^a h(x,a)\sigma_{rs}(x)dx \tag{5}$$

The residual stress field has been derived by neglecting the potentially present residual stress field from the manufacturing process prior to welding. The thermo-mechanical rolling process plastically deforms the steel and cools it in air. Thermal gradients in the material are kept low and it is expected that residual stress formation for this manufacturing process is low. This may not be true for quenched and tempered steel grades, that may be prone to significant thermal gradients over the thickness of the specimen, leading to more pronounced residual stress formation.

The results of one of the crack compliance experiments on the bead-on-plate welded specimen is shown in Figure 12 for both a plane stress and plane strain constraint configuration (Equation 4). It is noted that a peak tensile residual stress field of 210 MPa is present at the sub-surface region. The top side of the specimen is heated up and expands during the welding procedure. The cooler core of the specimen still has sufficient stiffness to oppose the defomation of the sub-surface region, resulting in a tensile stress at the top and a balancing compression stress at the core. The tensile stress at the bottom is due to some angular distortions in the welded specimens, introducing a bending moment which results in a tensile stress at the bottom side.

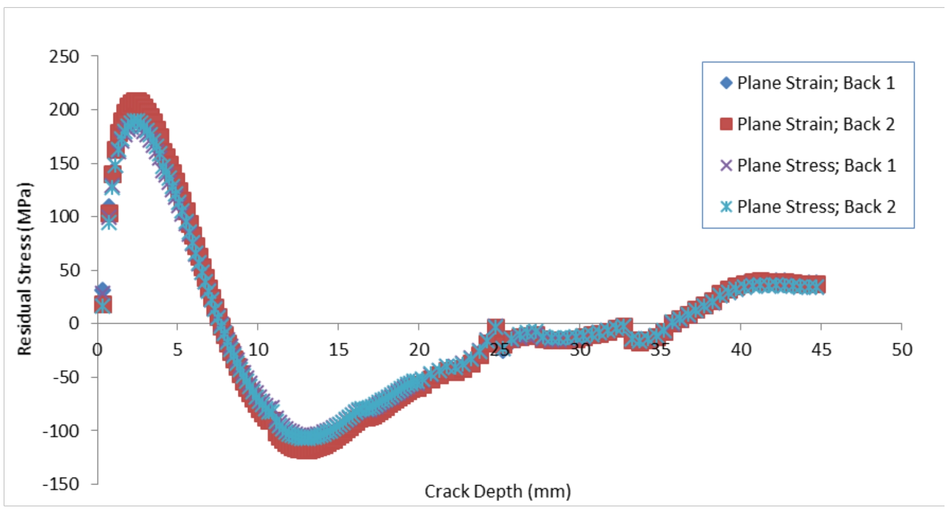

Figure 12 Through-thickness residual stress distribution of the bead-on-plate welded specimen

The mechanical analysis was decoupled from the thermal analysis in LS-DYNA by setting SOLN=2 in *CONTROL_SOLUTION. An fully coupled analysis is not usually necessary in welding simulation [10] because the heat generation during the plastic deformation of the metal is negligible. During completion of the analyses documented in this paper, it was concluded that the run time was reduced if the analyses are decoupled and that the residual stress field is hardly affected by doing so. The nodal temperature history resulting from the thermal analysis was input as nodal loads in the mechanical analysis.

The thermal expansion behavior of the steel determines the thermal strain development from the nodal temperature output of the thermal analysis. The current work only considers linear thermal expansion and neglects volumetric strain components which occur during solid-liquid and liquid-solid phase transformations of the steel at the appropriate temperature ranges. The thermal strains are transferred into stresses, using the temperature dependent stress-strain curves, Young’s modulus and Poisson ratio. This results in the formation of residual stresses and distortions in the welded specimen.

The material card MAT_270_CWM also includes annealing options. The plastic strains are reset to zero if the temperature exceeds a user defined temperature level. From that temperature level onwards, the material behaves as an ideal elastic-plastic material but experiences no evolution of plastic strains from the annealing temperature onwards. In the current work, recommendations from [11] were used in which the A1 and A3 temperature levels are used as an approximation for the annealing temperature. The A1 and A3 temperature levels at which the iron lattice structure starts and finishes the transformation from ferrite to austenite are 735 and 888.5 °C respectively.

The experimentally and numerically obtained residual stress distributions are compared in Figure 13. This figure shows the through thickness residual stress field, perpendicular to the weld direction, at 2mm laterally from the weld toe. The influence of the annealing function has been explicitly analyzed, showing one analysis result with and one without the annealing capability. The LS-DYNA output is in good agreement with the experimentally obtained residual stress field, validating the LS-DYNA capabilities in predicting residual stress field using computational welding mechanics. A contour plot of stress in the transverse direction, perpendicular to the weld direction, is shown in Figure 14.

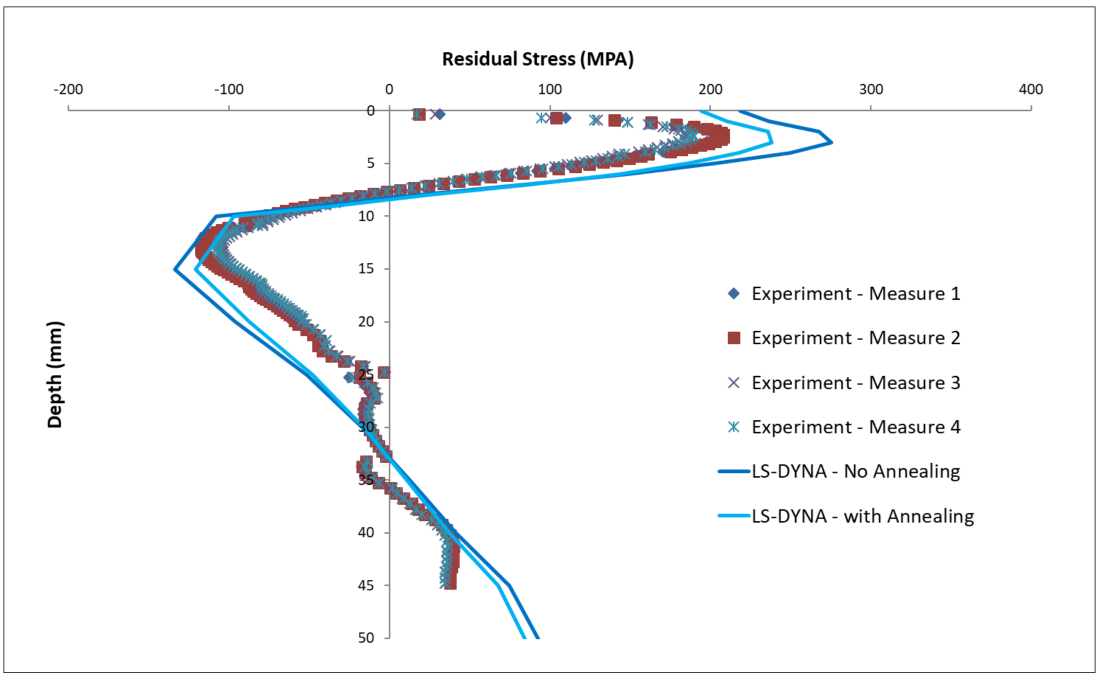

Figure 13 Residual stress distribution, numerically and experimentally, of the bead-on-plate specimens

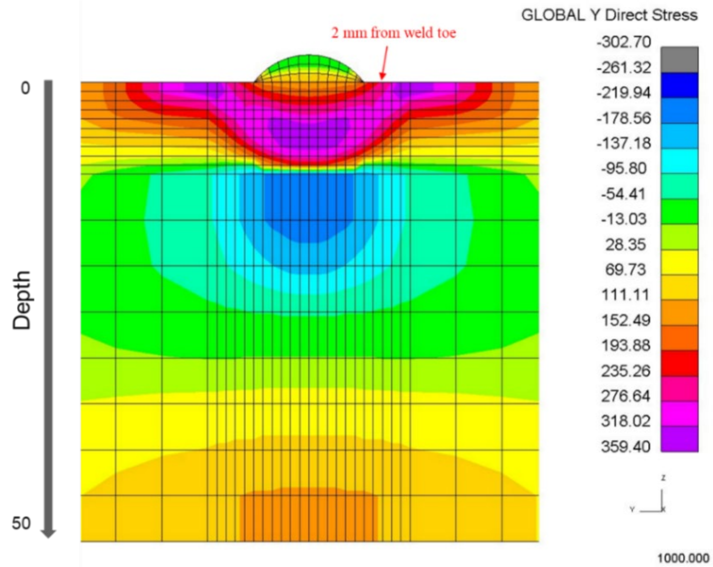

Figure 14 Contour plot of the residual stress distribution

This chapter examined the capabilities of LS-DYNA in predicting residual stress fields in a bead-on-plate welded specimen using computational welding mechanics. The input material data was obtained from JMatPro, assuming a uniform austenite grain size and cooling rate. The through thickness residual stress was examined by using the crack compliance method at 2mm from the weld toe. The experimental and numerical results are in good agreement, demonstrating the capabilities of LS-DYNA.

Conclusion

The current paper demonstrated the capabilities of LS-DYNA in computational welding mechanics. The material data was provided by a commercially available software package JMatPro, which provides LS-DYNA material cards. The thermo-mechanical decoupled analysis has been validated by means of experiments in which the numerical output corresponded well with the experimental results. The key conclusions of this paper are:

- JMatPro can offer reliable material properties which can be easily implemented in LS-DYNA.
- LS-DYNA has built-in capabilities for computational welding mechanics that are relevant and relatively straightforward to use.
- The welding specific input for the numerical simulations has a physical link with the actual welding procedure specification. This allows a user to set up welding simulations without needing extensive experimental test data as was used in this paper.
- LS-DYNA is capable of accurately predicting the temperature flow in a welded specimen.
- LS-DYNA is capable of providing an accurate representation of the residual stress field of a welded specimen.

A significant advantage of using computational welding mechanics is that it reduces the requirement for time consuming and expensive tests. Numerical techniques can be used to improve welding procedures or to predict the altered state of the structure due to the welding process to enable more reliable in-service strength and fatigue calculations to be completed. It also provides the user with more freedom to look at the effect of individual parameters on the formation of the undesirable side effects of welding, instead of verifying only one set of input parameters by testing.

Additional capabilities of LS-DYNA

The current paper examined a bead-on-plate welded specimen using a S355G10+M base material, which has been produced by gas metal arc welding. The key interests were the temperature flow and residual stress distribution. LS-DYNA and JMatPro offer additional capabilities in computational welding mechanics which increase the potential application of LS-DYNA across various industries. A few examples of additional capabilities are:

- The material card MAT_254 is a more advanced mechanical material card as opposed to MAT_270_CWM. This card includes the options of the latter card but offers additional phase transformation prediction options. The formation of austenite, ferrite, pearlite, bainite and martensite during a welding thermal cycle can be explicitly examined if one has the availability of TTT/CCT diagrams. These diagrams can be obtained using JMatPro. Studying the formation of hard and brittle zones can be interesting for the development of welding procedures and/or for structural integrity assessments. Arup is currently demonstrating the capabilities of LS-DYNA in this area.
- The welding simulations can be used to predict distortions and therefore welding procedures can be developed in which distortion is kept to a minimum.
- The Goldak volumetric heat source distribution is an often-applied representation of the heat input for arc welding procedures. The *BOUNDARY_WELD_TRAJECTORY card offers other heat source models that can be used for example in laser welding or electron beam welding applications.
- JMatPro offers material data for a wide range of alloys, including aluminum, steel and stainless-steel grades. The coupling between JMatPro and LS-DYNA is made easier as JMatPro offers LS-DYNA input decks that can be directly read in to the numerical software. This coupling increases the applicability of welding simulations for various welding applications.
- A welding simulation can be set up to study for example residual stresses, phase transformations or distortions. The results from the welding analysis can be used subsequently in mechanical or stability simulations in which it might influence the in-service loading capacity. The welding results may furthermore be used in structural integrity assessment e.g. fatigue and fracture.

References

[1] Goldak, J., Chaklavarti, A., Bibby, M., "A new finite element model for welding heat sources," *Metallurgical Transactions B,* vol. 15B, June 1984.

[2] Saunders, N., Guo, Z., Li, X., Miodownik, A.P., Schille, J-Ph., "Using JMatPro to model materials properties and behavior," *JOM,* pp. 60-65, 2003.

[3] Shan, X., Davies, C.M., Wangsdan, T., O'Dowd, N.P., Nikbin, K.M., "Thermo-mechanical modelling of a single-bead-on-plate weld using the finite element method," *International journal of pressure vessels and piping,* vol. 86, pp. 110-121, 2007.

[4] Gao, H., "PhD Thesis: Residual stress developments due to high-frequency post weld impact treatments for high-strength steels," TU Delft, Delft, 2014.

[5] Prime, M. B., "Experimental procedure for crack compliance (slitting) measurements of residual stress," Los Alamos National Laboratory, United States of America, 2003.

[6] Schindler, H.J., Cheng W., Finnie, I., "Experimental determination of stress intensity factors due to residual stresses," *Experimental mechanics,* vol. 37, pp. 272-277, 1997.

[7] Bueckner H.F., "A novel principe for the computation of stress intensity factors," Zeischrift fur angewandte methematik und mechanic volume 50, 1970.

[8] Wu, X., Carlsson, J., "Weight functions and stress intensity factor solutions," University of Michigan, United States of America, 1991.

[9] Shindler, H.J., Bertschinger, P., "Some steps towards automation of the crack compliance method to measure residual stress distributions," Swiss federal laboratories for materials testing and research, Dubendorf, Switserland, 1997.

[10] Goldak, J., Akhlaghi, M., "Computational welding mechanics," Springer, Ottawa, Canada, 2005.

[11] Lindstrom, R.M. , "DNV platform of computational welding mechanics, Document number: X-1732-13," 2013.